Redox Equilibria in Hydroxylamine Oxidoreductase. Electrostatic Control of Electron Redistribution in Multielectron Oxidative Processes†

Igor V. Kurnikov,*,‡ Mark A. Ratner,*,‡ and A. Andrew Pacheco*,§

Chemistry Department, Northwestern University, 2145 Sheridan Road, Evanston, Illinois 60208, and Department of Chemistry and Biochemistry, University of Wisconsin, 3210 North Cramer Street, Milwaukee, Wisconsin 53211

Received September 9, 2004; Revised Manuscript Received November 7, 2004

ABSTRACT: We report results of continuum electrostatics calculations of the cofactor redox potentials, and of the titratable group pK_a values, in hydroxylamine oxidoreductase (HAO). A picture of a sophisticated multicomponent control of electron flow in the protein emerged from the studies. First, we found that neighboring heme cofactors strongly interact electrostatically, with energies of 50−100 mV. Thus, cofactor redox potentials depend on the oxidation state of other cofactors, and cofactor redox potentials in the active (partially oxidized) enzyme differ substantially from the values obtained in electrochemical redox titration experiments. We found that, together, solvent-exposed heme 1 (having a large negative redox potential) and heme 2 (having a large positive redox potential) form a lock for electrons generated during the oxidation reaction The attachment of HAO's physiological electron transfer partner cytochrome c_{554} results in a positive shift in the redox potential of heme 1, and "opens the electron gate". Electrons generated as a result of hydroxylamine oxidation travel to heme 3 and heme 8, which have redox potentials close to 0 mV versus NHE (this result is in partial disagreement with an existing experimental redox potential assignment). The closeness of hemes 3 and 8 from different enzyme subunits allows redistribution of the four electrons generated as a result of hydroxylamine oxidation, among the three enzyme subunits. For the multielectron oxidation process to be maximally efficient, the redox potentials of the electron-accepting cofactors should be roughly equal, and electrostatic interactions between extra electrons on these cofactors should be minimal. The redox potential assignments presented in the paper satisfy this general rule.

Prokaryotes can extract energy from an astonishing range of oxidation−reduction reactions. Such prokaryotic respiratory processes play a critical role in shaping the chemical environment of the biosphere (*1*, *2*), and are carried out by highly efficient protein systems. In recent years, some understanding of the general principles of effective catalysis in bacterial multielectron redox processes has started to emerge. Indeed, spectacular progress has been achieved in elucidating the function of some of the critical bioenergetics systems, such as the photosynthetic reaction center, cytochrome *c* oxidase, and cytochrome bc_1. This progress has been fueled in large part by the appearance of atomic-resolution three-dimensional structures of these complex systems. For mechanistic aspects of enzyme function that are difficult to study experimentally, the structural information permits the application of quantitative simulation techniques. Herein, we report the results of continuum electrostatics calculations, used to simulate the reduction potentials of the heme cofactors from the enzyme hydroxylamine oxidoreductase (HAO),[1] obtained from the bacterium *Nm. europaea*. The ultimate goal of these calculations is to understand the control of electron flow in HAO, and its relevance to the enzyme's function.

The enzyme hydroxylamine oxidoreductase (HAO) from the autotrophic bacterium *Nm. europaea* is a periplasmic multi-heme-containing enzyme that catalyzes the four-electron oxidation of NH_2OH to NO_2^- (eq 1) (*3*−*5*).

$$NH_2OH + H_2O \rightarrow NO_2^- + 4e^- + 5H^+ \qquad (1)$$

This is the second of two steps by which NH_4^+ is oxidized to NO_2^- in *Nm. europaea*. The first step, oxidation of NH_4^+ to NH_2OH, is catalyzed by the enzyme ammonia monooxygenase (*5*, *6*). The net aerobic oxidation of NH_4^+ to NO_2^- is critical to *Nm. europaea*, which derives all its energy for growth from the process (*5*, *7*). As part of the biosphere's nitrogen cycle, the oxidation of NH_4^+ to NO_2^- also has enormous economic and ecological importance (*6*−*13*). Over the past 8 years, an increasing number of multi-heme-containing proteins have been isolated from the respiratory systems of a wide variety of microbial sources (*14*−*17*). In cases where the protein structures have been determined, the

† Funding was provided by the Chemistry Division of the National Science Foundation and the ONR.

* To whom correspondence should be addressed. I.V.K. and M.A.R.: Chemistry Department, Northwestern University, 2145 Sheridan Rd., Evanston, IL 60208; phone, (847) 467-4993; fax, (847) 491-7713; e-mail, igor@kurnikov.org (I.V.K.) and ratner@chem.northwestern.edu (M.A.R.). A.A.P.: Department of Chemistry and Biochemistry, University of Wisconsin, 3210 N. Cramer St., Milwaukee, WI 53211; phone, (414) 229-4413; fax, (414) 229-5530; e-mail, apacheco@uwm.edu.

‡ Northwestern University.

§ University of Wisconsin.

[1] Abbreviations: HAO, hydroxylamine oxidoreductase; NHE, normal hydrogen electrode; *Nm. europaea*, *Nitrosomonas europaea*; EPR, electron paramagnetic resonance.

10.1021/bi048060v CCC: $30.25
Published on Web 01/22/2005

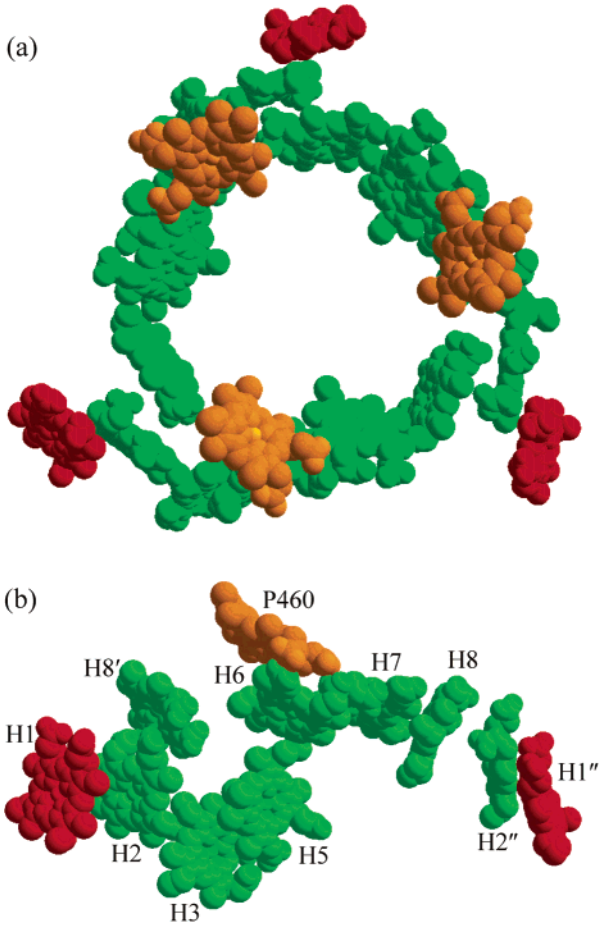

FIGURE 1: Heme arrangement in HAO: (a) in the full trimer and (b) in one subunit. The active site P_{460} heme is colored orange, and solvent-exposed heme 1 red. All other hemes (green) are buried within the protein matrix.

hemes have proven to be arranged in recurring motifs very similar to those found in HAO (*15*, *16*). Typically, the proteins are otherwise unrelated in function, size, or even folding pattern (*15*), but in all cases, the hemes are critical in electron transport and storage. Because of the vital role that microbial respiratory processes play in shaping the chemical environment of the biosphere (*1*, *2*), interest in the whole family of multi-heme proteins is considerable. We anticipate that our ongoing studies of HAO will provide valuable insights not just about HAO itself but also about other multi-heme proteins and multicofactor enzymes in general.

The purification to homogeneity of *Nm. europaea* HAO was first reported more than 20 years ago (*18*, *19*), and its crystal structure recently became available (*20*). A fascinating feature of HAO is its remarkable complexity. The enzyme is a homotrimer, with a molecular mass of 67 kDa per monomer. Each monomer contains seven *c*-type hemes, and a novel eighth heme known as P_{460} (Figure 1b). The Fe center of P_{460} has a vacant coordination site at which NH_2OH binds and is then oxidized (*20*−*24*). The remaining seven hemes are all six-coordinate, with two His ligands each, and are in the low-spin ferric state in the resting enzyme (*20*, *25*). Adjacent heme groups are spaced sufficiently close together to allow rapid electron transfer between their Fe centers, and the branched chain arrangement of the hemes (Figure 1) allows the electrons injected at P_{460} to be quickly transported from heme to heme over large distances (*20*, *25*). Moreover, heme 8 in each subunit lies sufficiently near hemes 1 and 2 of an adjacent subunit to possibly allow electron transfer between subunits (Figure 1a). Indeed, the 18-heme circle seen in the HAO trimer (Figure 1a) appears to be superbly designed to allow e^- entering at a single P_{460} to be rapidly distributed throughout the trimer.

Oxidation of NH_4^+ to NO_2^- by O_2 yields much less energy than oxidation of organic foodstuffs. Because this is the only process from which *Nm. europaea* can extract usable energy from the surroundings (*6*, *9*, *10*), it is likely that HAO is optimized to maximize utilization of the free energy released in the process. One of the crucial aspects in the design of HAO is the tuning of the heme standard reduction potentials. These will strongly influence the energetics of individual steps in hydroxylamine oxidation. They will also affect the kinetics of electron transfer events within HAO, and in the complex of HAO with its physiological electron acceptor, cytochrome c_{554} (*6*, *26*, *27*). Reduction potentials corresponding to all eight unique HAO hemes have been resolved in spectropotentiometric titrations (*28*, *29*), and five of eight of these potentials have been assigned to specific hemes in the structure (*30*, *31*). However, spectropotentiometric titrations yield equilibrium potentials for the HAO hemes. That is, the standard reduction potential of any given heme is obtained only after higher-potential hemes have been reduced. Because the HAO hemes are in the proximity of the enzyme, the oxidation state of any one heme may have a strong effect on the potentials of adjacent hemes. Consequently, the heme potentials during nonequilibrium events, such as the movement of a single e^- through the molecule, may differ substantially from the experimentally measurable equilibrium potentials. Herein, we have taken advantage of the availability of the atomic-resolution three-dimensional structure (*20*) to simulate quantitatively the reduction potentials of HAO, under both equilibrium and nonequilibrium conditions. The nonequilibrium simulations are more physiologically relevant, but the equilibrium simulations are essential because they yield numbers that can be directly compared to the published experimental reduction potentials (*28*, *29*) to verify their validity.

METHODS

Our approach to computing the redox potentials of hemes in HAO is similar to that used previously (*32*−*35*). It is based on calculating the difference in transfer free energies of the oxidized and reduced cofactors, when moving the cofactor from a water solution to the protein environment, using a numerical solution of the linearized Poisson−Boltzmann equation (eq 2).

$$\vec{\nabla}\cdot[\epsilon(\vec{r})\nabla\vec{\varphi}(\vec{r})] = -4\pi\rho(\vec{r}) + \kappa^2\varphi(\vec{r}) \qquad (2)$$

In this equation, ϵ, φ, ρ, and κ represent the local dielectric constant, the electrical potential, the charge density, and the ionic atmosphere screening factor, respectively. Preliminary calculations indicated that the computed standard reduction potentials of the HAO hemes depend strongly on the protonation state of surrounding titratable groups, such as the heme propionates (see also refs *33* and *36*). Thus, reliable estimates of the heme reduction potentials can only be

obtained by simultaneously analyzing the protonation equilibrium of titratable groups, characterized by their pK_a values.

We describe the dependence of the system's free energy G on the protonation and redox states of the chemical groups within the system in eq 3. In this equation, components x_i of system state vector **x** have values of 0 and 1, and describe the states of the titratable and redox groups in the system. The standard state of the system (with state vector **x** having all components equal to 0) has all redox groups oxidized, and titratable groups in the protonation states that are dominant for the isolated residues in water at neutral pH.

$$G(\mathbf{x}) = \sum_i W_{ii} x_i + \sum_{i>j} W_{ij} x_i x_j \quad (3)$$

Interaction energies W_{ij} between groups in eq 3 are found using Poisson−Boltzmann calculations and eq 4:

$$W_{ij} = \sum_k \Delta q_k^i \Delta \phi_k^j \quad (4)$$

where Δq_k^i is the change in electric charge in the kth atom of the ith titratable group and $\Delta \varphi_k^j$ is the change in electrostatic potential on this atom when the jth group is reduced (or changes its protonation state).

Diagonal matrix elements are computed with eq 5a (for titratable groups) and eq 5b (redox groups):

$$W_{ii} = kT(\mathrm{pH} - \mathrm{p}K_a^{\mathrm{solvent}}) \ln 10 + (\Delta G_{i,\mathrm{protein}}^{\mathrm{protonation}} - \Delta G_{i,\mathrm{solvent}}^{\mathrm{protonation}}) \quad (5a)$$

$$W_{ii} = e(E_{\mathrm{ext}} - E_{i,\mathrm{solvent}}^0) + (\Delta G_{\mathrm{protein}}^{\mathrm{reduction}} - \Delta G_{\mathrm{solvent}}^{\mathrm{reduction}}) \quad (5b)$$

The first term in eq 5a depends on the pH of the system and on the pK_a value of the reference molecule (an isolated amino acid) in the solvent. The second term, computed using Poisson−Boltzmann calculations, is the change in the protonation free energy of a titratable group upon transfer from the solvent to a protein environment (with other groups in standard protonation and redox states).

The first term in eq 5b depends on the equilibrium electrode potential of the system and the redox potential of an isolated redox group in the solvent. The experimentally known standard reduction potential of FeP(Im)$_2$ (Fe-protoporphyrin IX bisimidazolate) in water (*37*, *38*) was used as a reference. The second term, computed using Poisson−Boltzmann calculations, is the change in the reduction free energy of the redox group when it is transferred from the solvent to the protein environment.

To compute the average population of alternative redox and protonation states for a given set of external electrode potentials (E_{ext}) and pH values, we used two methods. The first method is a mean-field approach in association with the free energy expression (eq 3). If one assumes that probabilities of the alternative states of the ith titratable group depend only on the average population of alternative states of the other chemical groups, then the average population of the states of the group can be expressed as

$$\langle x_i \rangle = \frac{\sum_{\alpha=0,1} \alpha \exp[-G(\langle \mathbf{x} \rangle, x_i = \alpha)/k_B T]}{\sum_{\alpha=0,1} \exp[-G(\langle \mathbf{x} \rangle, x_i = \alpha)/k_B T]} = \frac{1}{\exp[(W_{ii} + \sum_{i \neq j} W_{ij} \langle x_j \rangle)/k_B T] + 1} \quad (6)$$

A nonlinear system of equations (eq 6) was solved using an iterative overrelaxation method for a given pH and external redox potential, and finally, the redox potentials of the heme groups were found using eq 7 derived from eqs 3 and 6:

$$E_i^0(E_{\mathrm{ext}}, \mathrm{pH}) = E_{i,\mathrm{solvent}}^0 - (\Delta G_{\mathrm{protein}}^{\mathrm{reduction}} - \Delta G_{\mathrm{solvent}}^{\mathrm{reduction}} + \sum_{i \neq j} W_{ij} \langle x_j \rangle)/\mathrm{e} \quad (7)$$

It can be seen from eq 7 that any given heme redox potential depends not only on pH but also on the external electrode potential that defines the equilibrium population of the remaining heme redox states. Equilibrium midpoint potentials $E^{1/2}$ of the hemes (the external electrode potential that causes a given heme population to be 50% in the reduced state) obtained in redox titration experiments were found by solving eq 8.

$$E_i^{1/2} = E_i^0(E_{\mathrm{ext}}, \mathrm{pH}) = E_{\mathrm{ext}} \quad (8)$$

The second approach we used to simulate redox titration curves of HAO involved Monte Carlo simulations with a spin−lattice Hamiltonian of eqs 3−5 (*39*, *40*). A Metropolis sampling scheme was used. An elemental Monte Carlo step involved an attempt to change the redox or titration state x_i of group i. We successively tried to change the states of all titratable and redox groups in sequence, and used 10^6 passes over each group of the protein (total number of MC steps equal 10^6 times the number of groups) to compute average populations of groups and given pH and E_{ext}. We found this number of MC steps to be sufficient for convergence of computed average populations with an accuracy of ~1% or better.

RESULTS

As seen from eq 7, the redox potential of any one heme cofactor depends on the average populations of surrounding redox-active and/or titratable groups. Consequently, the midpoint potentials obtained in redox titration experiments do not necessarily coincide with the redox potentials of cofactors in partially oxidized HAO, as it would be found during the enzyme catalytic cycle. However, we will simulate equilibrium redox titration curves, to connect our calculations to experimentally obtainable data. Protonation states of titratable groups also affect the redox potentials of the cofactor. To illustrate this point, we first compute the pK_a values of titratable groups for the protein in a fully oxidized state. Table 1 shows pK_a values for His (not including those bound to the hemes) and heme propionates for two values of the protein dielectric constant ($\epsilon_{\mathrm{in}} = 4.0$ and 10.0). While an ϵ_{in} of 4.0 more realistically describes the expected low-

Table 1: pK_a Values of Titratable His and Heme Propionates for Fully Oxidized HAO, Obtained for Two Plausible Values of the Average Dielectric Constant (see the text for details)

	$\epsilon_{in} = 4.0$	$\epsilon_{in} = 10.0$	qualitative conclusion
His38	6.50	6.87	partially protonated
His268	7.56	9.19	active site His (protonation will depend on heme 3)
His395	7.63	7.89	partially protonated
His454	−3.8	6.18	unprotonated
heme 1 A	−6.67	1.37	unprotonated
heme 1 D	8.48	6.88	partially protonated
heme 2 A	−6.78	−1.02	unprotonated
heme 2 D	15.0	10.6	protonated (H-bond to Tyr57 CO)
heme 3 A	4.06	4.65	unprotonated
heme 3 D	14.10	7.67	partially protonated (H-bond to heme 5 propionate)
heme 4 A	6.56	5.42	unprotonated
heme 4 D	11.84	9.64	protonated (H-bond to heme 6 propionate)
heme 5 A	3.57	4.13	unprotonated
heme 5 D	1.86	3.08	unprotonated
heme 6 A	11.70	8.77	protonated (H-bond to heme 4 propionate)
heme 6 D	16.36	11.09	protonated (H-bond to heme 4 propionate)
heme 7 A	1.06	5.75	unprotonated (H-bond to propionate D)
heme 7 D	12.81	6.19	partially protonated (H-bond to propionate A)
heme 8 A	−4.87	3.37	unprotonated
heme 8 D	7.19	5.74	unprotonated (may be partially protonated)

Table 2: Matrix of Electrostatic Interactions between Extra Electrons on HAO Hemes (potentials given in millivolts)[a]

	heme 8 p	heme 1	heme 2	heme 3	P_{460}	heme 5	heme 6	heme 7	heme 8
heme 8 p	**31**	14	38	13	16	16	22	9	4
heme 1	14	**−133**	**66**	9	2	5	3	1	1
heme 2	38	**65**	**+264**	46	7	23	13	5	2
heme 3	13	9	46	**+52**	5	**73**	15	7	3
P_{460}	16	2	7	5	**−153**	13	**64**	25	6
heme 5	16	5	23	**73**	13	**−113**	52	23	8
heme 6	22	3	12	15	**64**	52	**−106**	79	15
heme 7	9	1	5	7	25	23	**79**	**−27**	**51**
heme 8	4	1	2	3	6	8	15	**51**	**31**

[a] Computed with an ϵ_{in} of 10.0 and an ionic strength of 0.1 M. Diagonal matrix elements (heme redox potentials for a fully oxidized enzyme) are underlined. Off-diagonal heme−heme interactions larger than 50 mV are in bold type.

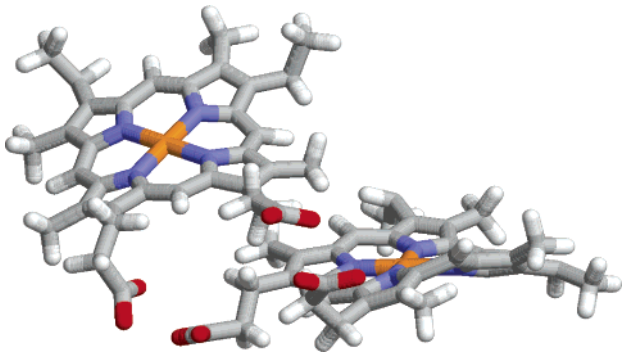

FIGURE 2: Hemes 4 and 6 in the crystal structure of HAO. Hydrogen bonding is evident for at least one pair of propionates. Calculations predict these propionates to be protonated (pK_a > 8.0).

dielectric environment inside the proteins, calculations of pK_a values with an ϵ_{in} of 10.0 typically give better results for continuum electrostatics calculations of pK_a of protein surface residues (*40*, *41*). This is probably because the mobilities of side chains exposed to solvent are indirectly taken into account by the larger values of ϵ_{in} (*42*−*44*). Examination of Table 1 indicates that calculations predict some of the heme propionates to be protonated. Figure 2 shows hemes 4 and 6 that have protonated propionates according to computed pK_a values. Indeed, X-ray data show that the minimal distances between the carboxylate oxygens of the two heme propionates are 2.8 and 3.2 Å, respectively, strongly indicating the existence of hydrogen bonds between two pairs of propionates, and thus corroborating their protonated status (*20*).

In the next step, we analyzed the energetics of the heme redox states. The results of the analysis computed for a protein dielectric constant of 10.0 and an ionic strength of 0.1 M are presented in Table 2. The diagonal of Table 2 presents the redox potentials of the hemes in the fully oxidized state of the protein, computed by taking into account heme desolvation and interactions with other protein charges (all redox potentials in the paper reported vs the NHE reference). The off-diagonal elements of Table 2 give W_{ij} values of eqs 3−7 (interactions between extra charges on the hemes). Table 2 shows that the electrostatic interactions between extra charges on adjacent HAO cofactors are quite strong, and are as high as 80 mV (≈3 kT) for calculations with an ϵ_{in} of 10.0. Calculations with an ϵ_{in} of 4.0 give even larger values for these interactions (up to 170 mV).

Because many of the heme cofactors are located deep inside the protein, it is expected that calculations with an ϵ_{in} of 4.0 will be quite realistic. On the other hand, even the lower estimates of these electrostatic interactions, obtained in calculations with an ϵ_{in} of 10.0, allow an immediate challenge to the assignment of hemes 3 and 5 as those reduced at applied potentials of 10 and −10 mV (*31*). If one of these hemes is titrated at a redox potential of 10 mV [and our calculations agree with the spectroscopic assignment of this midpoint redox-potential to heme 3 (*31*)], then the

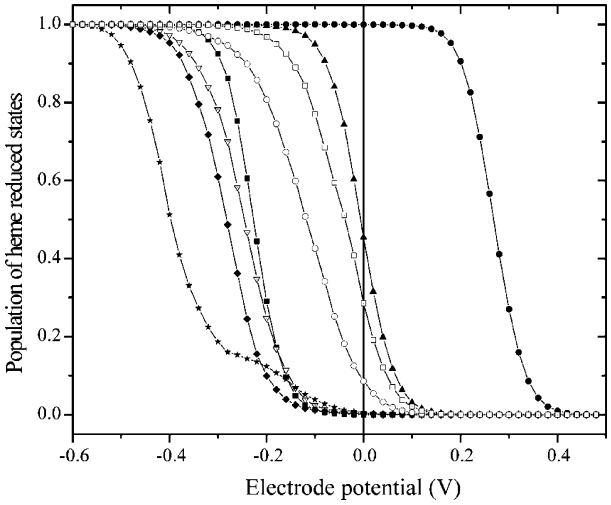

FIGURE 3: Simulation of a redox titration of HAO. The average populations of reduced heme states are given as functions of a given external electrode potential. From highest potential to lowest: (●) heme 2, (▲) heme 3, (□) heme 8, (○) heme 7, (■) heme 1, (▽) P_{460}, (◆) heme 5, and (★) heme 6.

redox potential of the neighboring heme (heme 5) will be shifted at least 73 mV due to electrostatic repulsion between hemes [this phenomenon is often termed coulomb blockade (*45*, *46*)]. Thus, heme 5 cannot be the heme reduced at 10mV! Instead, the next electron added to the protein subunit should occupy a more distant heme, which we argue below should be heme 8.

From Table 2, it is also very clear that the highest-potential heme is heme 2 (Figure 1), and this cofactor is reduced first in a potentiometric titration. Its computed redox potential of 264 mV with all hemes oxidized agrees very well with the experimental value of 288 mV that was obtained in potentiometric titrations for the highest-potential heme of HAO. This is more than 200 mV more positive than the next-highest computed redox potential, with a value of 52 mV for heme 3.

We simulated the HAO potentiometric titration using eq 7, by shifting the potential of the external electrode, and then computing the average population of the HAO hemes and titratable groups using Monte Carlo simulations. Titration curves giving the average redox states for the HAO heme populations are presented in Figure 3. The calculations successfully predicted the experimentally obtained values of the first, second, and third midpoint potentials of HAO. In agreement with EPR assignment (*31*), the calculations show that heme 3 accepts the second electron; however, calculations also predict that the third electron goes to heme 8, contradicting a previous assignment that sets heme 5 as the acceptor of the third electron (*31*). As will be shown below, these conclusions have very important consequences for the predicted mechanism of HAO action.

Our calculations predict that the fourth heme to be reduced in a redox titration is heme 7. This is in agreement with the assignment from potentioemetric experiments (*31*). The calculated order of reduction of the low-potential hemes (1, 4, 5, 6) becomes progressively less reliable. This is partially because of predicted strong cooperative effects that change the individual redox potentials as the heme electron population, and concomitant electrostatic repulsions, increase. It can be seen from Figure 3 that in simulations heme 6 became

Table 3: Simulated Spectropotentiometric Titration (pH 7), Showing the Predicted Order of Heme Reduction Compared to the Experimentally Based Assignments (*31*)[a]

	heme reduced	$E°$(calcd) (mV)	E_m(exptl) (mV)	previous assignment
electron 1	heme 2[b]	+270	+280	−
electron 2	heme 3[b]	−5	+10	heme 3[b]
electron 3	heme 8[c]	−39	−10	heme 5
electron 4	heme 7	−120	−160	heme 7
electron 5	heme 1	−225	−190	heme 6[b]
electron 6	P_{460}	−246	−260	−
electron 7	heme 5	−282	−265	P_{460}[b]
electron 8	heme 6	−398	−412	−

[a] Where appropriate, the confidence of each assignment is indicated. [b] Definitive assignment. [c] Probable assignment. Hemes 7 and 8 could switch.

Table 4: Computed Reduction Potentials of the HAO Hemes in the Fully Oxidized and Partially Reduced Enzyme[a]

	$E°$ (mV)		
	fully oxidized	heme 2 reduced	hemes 2, 3, and 8 reduced
heme 1	−133	−194	−213
heme 2	+264	+264	+203
heme 3	+52	+2	−11
P_{460}[b]	−153	−159	−186
heme 5	−113	−127	−208
heme 6	−106	−116	−170
heme 7	−27	−44	−94
heme 8	31	−10	−38

[a] These electron configurations are the most physiologically relevant for the enzyme. [b] Potential shifted by +180 mV.

substantially reduced at a potential of approximately −200 mV, in apparent agreement with the assignment of the experimental −190 mV midpoint potential to this heme (*30*, *31*). However, at more negative external electrode potentials, the simulated reduction level of heme 6 stabilizes, and ultimately, this heme is predicted to be completely reduced only below −400 mV. Hemes 5 and 6 are computed to be almost isopotential at high positive external electrode potentials, when all hemes are oxidized (see Tables 2 and 4). Small variations in the intrinsic potentials of hemes 5 and 6 (20−40 mV) resulted in large variations in the predicted titration curves; therefore, the order of reduction of these hemes is rather uncertain from calculations.

To obtain more confidence in the results of redox equilibrium simulations, we also computed redox titration curves for cytochrome c_{554}. This protein is the physiological ET partner for HAO, and has a similar heme arrangement (*16*). The titration curve is shown in Figure 4. Encouragingly, initial calculations successfully showed that the more exposed hemes I and II are reduced at more positive redox potentials than the more buried hemes III and IV, as observed experimentally (*47*). To match the titration potentials of hemes I and II that are experimentally known to be equal, we shifted the standard redox potential of the five-coordinate, high-spin heme II by 0.18 V. We also used this shift for the high-spin P_{460} while simulating redox titration curves of HAO. With this correction, we realized very good agreement for titration curves of all four hemes of cytochrome c_{554} (Figure 4). It is important to emphasize that the low titration potential of heme III, and even lower potential of heme IV, are to a large extent due to the repulsion between extra electrons present in the heme pool when these hemes are

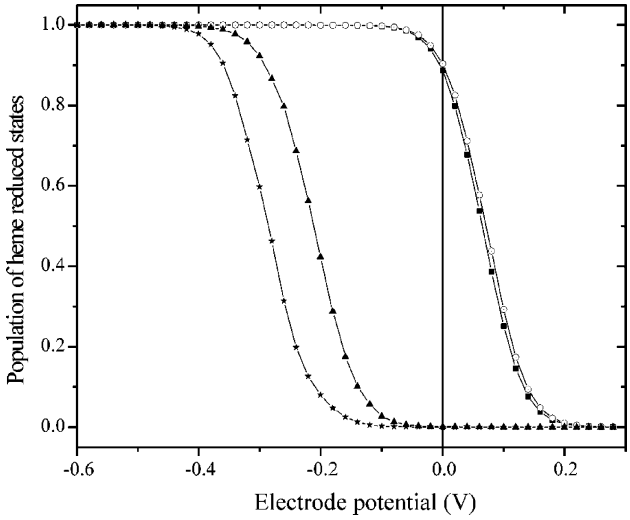

FIGURE 4: Simulated redox titration of cytochrome c_{554}. The average populations of reduced heme states are given as functions of a given external electrode potential. From highest potential to lowest: (○) heme I, (■) heme II, (▲) heme III, and (★) heme IV.

titrated. When all hemes are oxidized, the computed redox potentials of hemes III and IV are much more positive (approximately −100 mV). Thus, electrons can rather easily travel from heme I to heme II when cytochrome c_{554} is in the complex with HAO, and cytochrome c_{554} can readily accept two electrons from HAO.

DISCUSSION

Electrostatic analysis of redox equilibria in the multi-heme enzyme HAO has revealed a complicated scheme for protein control of electron transfer during the multi-electron oxidation of NH_2OH. Calculations show that the highest-potential HAO cofactor is heme 2. In fact, the potential of this heme is higher than those of the two highest-potential hemes on cytochrome c_{554} [47 mV (*26*)], which serves as the physiological electron acceptor for HAO. This suggests that heme 2 will probably stay reduced at all times under physiological conditions, and the first two electrons generated as a result of hydroxylamine oxidation will be transported to hemes 3 and 8. When only heme 2 is reduced, hemes 5−7 have redox potentials close in magnitude (∼100 mV more negative) to those of hemes 3 and 8, and should present a minimal obstacle to electron flow through the enzyme (Tables 2 and 4).

The next two electrons generated in the engaged active site of HAO will have no place to go, as hemes 2, 3, and 8 will be reduced, and the potentials of hemes 5 and 7 will then be too negative by ∼100 mV to accept the electrons (Table 4). However, hemes 3 and 8 are nearly isopotential with hemes 8 and 3 of the neighboring subunits (hereafter denoted hemes 8′ and 3′, respectively), and electrons can easily migrate there to allow hemes 3 and 8 from the active enzyme subunit to accept the next two electrons generated in the NH_2OH oxidation reaction. This suggestion is illustrated in Figure 5, and provides at least one important role for the availability of two electron migration paths leading away from the active site of HAO.

Another very interesting conclusion that can be drawn from the simulated redox potentials of the HAO cofactors is a possible role for solvent-exposed heme 1, in conjunction with high-potential heme 2, in the regulation of electron

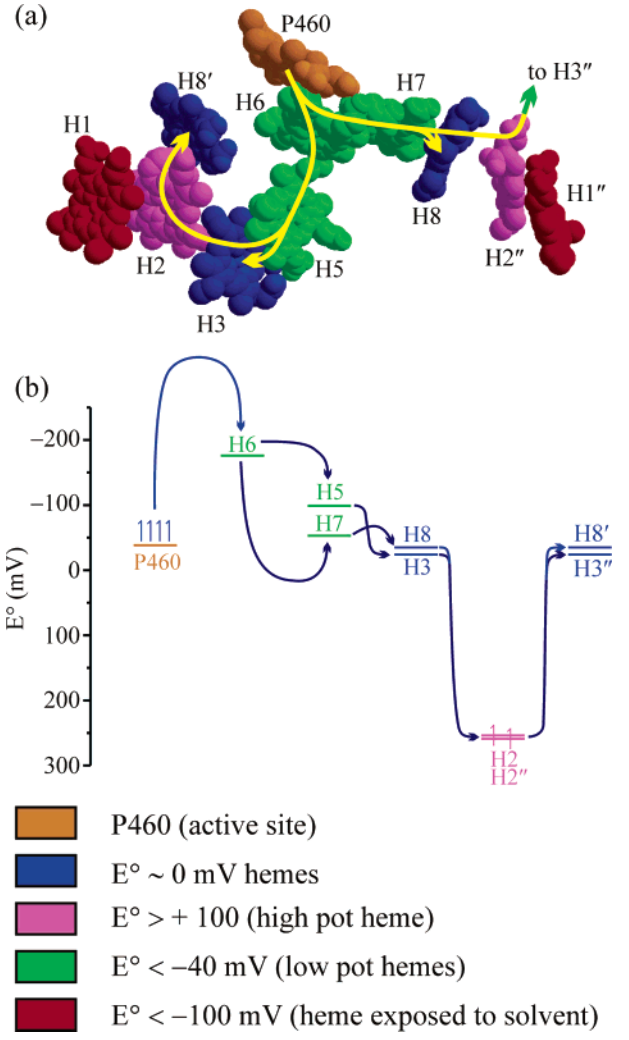

FIGURE 5: (a) Pathways available to electrons injected into P_{460} during NH_2OH oxidation. (b) Energy barriers to electron flow when only heme 2 is reduced. Hemes are color-coded according to their redox potentials.

transfer from reduced HAO to external oxidizing agents. Calculations predict (see Table 3) that in equilibrium redox titrations heme 1 is reduced after hemes 2, 3, 7, and 8, at the rather negative applied potential of −225 mV. One can see from Figure 6 that with these redox potential assignments, positive potential heme 2 and negative potential heme 1 will form an electrostatic lock for electrons generated in hydroxylamine oxidation, and located on hemes 3 and 8 with a redox potential of ∼0 mV. However, when HAO and cytochrome c_{554} come together during physiological ET (*27*), the potential of heme 1 is predicted to increase significantly (by ∼100 mV) due to desolvation of heme 1, and neutralization of the exposed heme 1 propionate, by the incoming cytochrome c_{554}. Such an increase in potential has been observed experimentally in cytochrome b_5, which has a solvent-exposed heme in an environment similar to that of HAO heme 1, when this protein interacts with large cations such as polylysine (*48*, *49*). A predicted practical consequence of the "tunability" of the HAO heme 1 potential is that electron efflux to the physiological acceptor cytochrome c_{554} will be considerably faster than efflux to even very powerful nonphysiological oxidants (*50*−*52*).

In addition to being tuned by the binding of cytochrome c_{554}, the heme 1−heme 2 lock will also be tuned by the

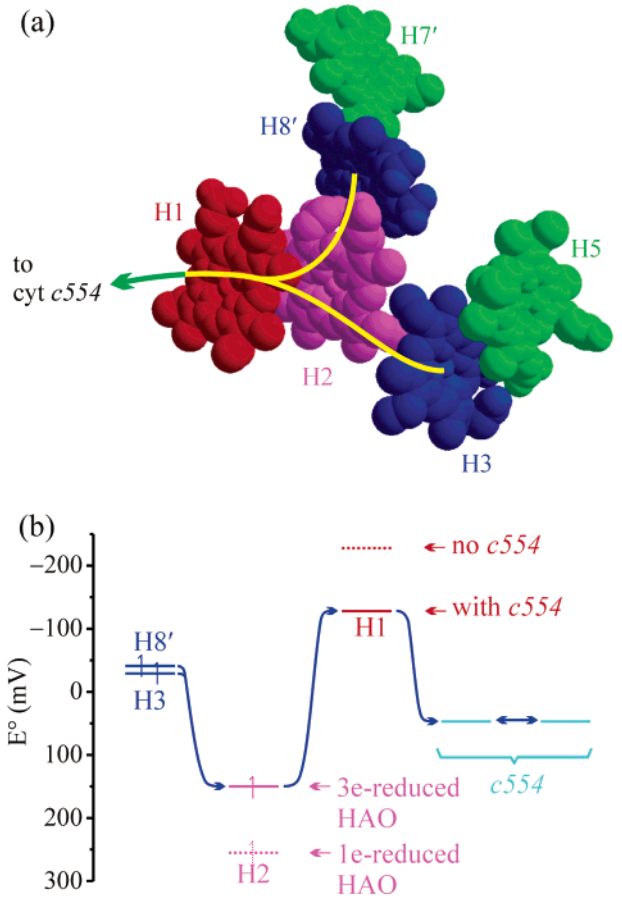

FIGURE 6: Oxidation of HAO by cytochrome c_{554}. The potential of the solvent-exposed heme is expected to increase by ~100 mV upon formation of the HAO−c_{554} complex, primarily due to desolvation of the heme 1 microenvironment. Note that the potential of heme 2 also becomes more negative when hemes 3 and 8 are reduced, which further lowers the energy barrier to ET from heme 2 to heme 1.

oxidation state of heme 3, as shown in Figure 6. When heme 3 is oxidized and heme 2 is reduced, the potential difference between hemes 1 and 2 will be maximized, thus making it especially unlikely that heme 2 will be oxidized by external agents. When heme 3 is reduced, the potential of heme 2 will be lowered by ~100 mV, thus coming closer to the potential of heme 1 and decreasing the energy barrier to electron efflux. Together, the binding of cytochrome c_{554} and the reduction of heme 3 will decrease the barrier from almost 500 mV uphill to less than 300 mV, which will greatly decrease the rate of electron efflux from HAO. The overall reduction of cytochrome c_{554} by a three-electron-reduced subunit of HAO can be visualized as a concerted process whereby the transfer of an electron from heme 2, uphill to heme 1, and further to cytochrome c_{554}, is accompanied by the (near) simultaneous downhill transfer of an electron from heme 3 to heme 2.

In agreement with the previously reported spectropotentiometric titrations (*28*), the computed simulation shows that four of the HAO hemes will be reduced at very low applied potentials. A robust and important conclusion of the simulation is that the apparent very negative midpoint potentials of these hemes are due to strong electrostatic repulsion by the previously reduced neighboring hemes. In the fully oxidized enzyme, theory predicts that no heme will have a redox potential below −150 mV (Tables 2 and 4). Even when the HAO subunits are reduced by one to three electrons, as they will be during catalytic turnover, the thermodynamic barriers to electron transport from the active site to electron-accepting hemes (predicted to be hemes 3 and 8) will be quite low (Table 4), allowing for sufficiently fast electron transport through the enzyme (*50*, *51*).

The continuum electrostatic analysis presented herein is relatively crude, and higher accuracy in calculations of the heme redox potentials and titratable group pK_a values will be achieved in future studies by incorporating explicit consideration of the protein dynamics. Nevertheless, even the crude analysis has provided important insights, including an important general design principle for enzyme systems that simultaneously handle multiple electrons within multiple redox-active sites. To achieve maximal efficiency in the conversion of chemical energy into electrical potential energy, the electron-accepting cofactors of the enzyme should have minimal electrostatic interactions. Otherwise, the electron population of some cofactors will affect the accepting and/or donating redox potentials of other cofactors, and losses in redox energies will occur when electrons are collected from the enzyme by subsequent electron transport proteins. Deciphering the mechanisms of electron transport control during HAO catalytic turnover will ultimately help in understanding the mechanisms of other enzymes that catalyze multi-electron oxidation−reduction reactions, and will also provide guidance in the design of artificial catalytic systems.

REFERENCES

1. Ehrlich, H. L. (2002) *Geomicrobiology*, Marcel Dekker, New York.
2. Fenchel, T., King, G. M., and Blackburn, T. H. (1998) *Bacterial Biogeochemistry*, 2nd ed., Academic Press, London.
3. Hooper, A. B., and Nason, A. (1965) Characterization of hydroxylamine-cytochrome *c* reductase from chemoautotrophs *Nitrosomonas europaea* and *Nitrosocystis oceanus*, *J. Biol. Chem. 240*, 4044−4057.
4. Andersson, K. K., and Hooper, A. B. (1983) O_2 and H_2O are each the source of one O in NO_2^- produced from NH_3 by *Nitrosomonas*: N-15-NMR evidence, *FEBS Lett. 164*, 236−240.
5. Ferguson, S. J. (1998) Nitrogen cycle enzymology, *Curr. Opin. Chem. Biol. 2*, 182−193.
6. Hooper, A. B. (1989) Biochemistry of the Nitrifying Lithoautotrophic Bacteria, in *Autotrophic Bacteria* (Schlegel, H. G., and Bowien, B., Eds.) pp 239−265, Science Tech Publishers, Madison, WI.
7. Prince, R. C., and George, G. N. (1997) The remarkable complexity of hydroxylamine oxidoreductase, *Nat. Struct. Biol. 4*, 247−250.
8. Kroneck, P. M. H., Beuerle, J., and Schumacher, W. (1992) Metal Dependent Conversion of Inorganic Nitrogen and Sulfur Compounds, in *Metal Ions in Biological Systems* (Sigel, H., and Sigel, A., Eds.) pp 455−505, Marcel Dekker, New York.
9. Wood, P. M. (1988) Monooxygenase and free radical mechanisms for biological ammonia oxidation, in *The Nitrogen and Sulfur Cycles* (Cole, J. A., and Ferguson, S. J., Eds.) pp 219−243, Cambridge University Press, New York.
10. Bock, E., Koops, H.-P., Harms, H., and Ahlers, B. (1991) The biochemistry of nitrifying organisms, in *Variations in Autotrophic Life* (Shively, J. M., and Barton, L. L., Eds.) pp 171−200, Academic Press, San Diego.
11. Schlegel, H. G. (1981) Microorganisms involved in the nitrogen and sulfur cycles, in *Biology of Inorganic Nitrogen and Sulfur* (Bothe, H., and Trebst, A., Eds.) pp 3−12, Springer-Verlag, New York.
12. *Biological Nitrogen Fixation* (1994) pp 6−32, National Academy Press, Washington, DC.
13. Burns, R. C., and Hardy, R. W. F. (1975) *Nitrogen Fixation in Bacteria and Higher Plants*, Springer-Verlag, New York.

14. Einsle, O., Messerschmidt, A., Stach, P., Bourenkov, G. P., Bartunik, H. D., Huber, R., and Kroneck, P. M. H. (1999) Structure of cytochrome *c* nitrite reductase, *Nature 400*, 476−480.
15. Leys, D., Meyer, T. E., Tsapin, A. S., Nealson, K. H., Cusanovich, M. A., and Van Beeumen, J. J. (2002) Crystal structures at atomic resolution reveal the novel concept of "electron-harvesting" as a role for the small tetraheme cytochrome *c*, *J. Biol. Chem. 277*, 35703−35711.
16. Iverson, T. M., Arciero, D. M., Hsu, B. T., Logan, M. S. P., Hooper, A. B., and Rees, D. C. (1998) Heme packing motifs revealed by the crystal structure of the tetra-heme cytochrome *c*554 from *Nitrosomonas europaea*, *Nat. Struct. Biol. 5*, 1005−1012.
17. Leys, D., Tsapin, A. S., Nealson, K. H., Meyer, T. E., Cusanovich, M. A., and Van Beeumen, J. J. (1999) Structure and mechanism of the flavocytochrome *c* fumarate reductase of *Shewanella putrefaciens* MR-1, *Nat. Struct. Biol. 6*, 1113−1117.
18. Hooper, A. B., Maxwell, P. C., and Terry, K. R. (1978) Hydroxylamine oxidoreductase from *Nitrosomonas*: Absorption-spectra and content of heme and metal, *Biochemistry 17*, 2984−2989.
19. Yamanaka, T., Shinra, M., Takahashi, K., and Shibasaka, M. (1979) Highly purified hydroxylamine oxidoreductase derived from *Nitrosomonas europaea*, *J. Biochem. 86*, 1101−1108.
20. Igarashi, N., Moriyama, H., Fujiwara, T., Fukumori, Y., and Tanaka, N. (1997) The 2.8 Å structure of hydroxylamine oxidoreductase from a nitrifying chemoautotrophic bacterium, *Nitrosomonas europaea*, *Nat. Struct. Biol. 4*, 276−284.
21. Hooper, A. B., and Terry, K. R. (1977) Hydroxylamine Oxidoreductase from *Nitrosomonas*: Inactivation by Hydrogen Peroxide, *Biochemistry 16*, 455−459.
22. Hendrich, M. P., Logan, M., Andersson, K. K., Arciero, D. M., Lipscomb, J. D., and Hooper, A. B. (1994) The Active-Site of Hydroxylamine Oxidoreductase from *Nitrosomonas*: Evidence for a New Metal Cluster in Enzymes, *J. Am. Chem. Soc. 116*, 11961−11968.
23. Logan, M. S. P., Balny, C., and Hooper, A. B. (1995) Reaction with cyanide of hydroxylamine oxidoreductase of *Nitrosomonas europaea*, *Biochemistry 34*, 9028−9037.
24. Logan, M. S. P., and Hooper, A. B. (1995) Suicide inactivation of hydroxylamine oxidoreductase of *Nitrosomonas europaea* by organohydrazines, *Biochemistry 34*, 9257−9264.
25. Arciero, D. M., and Hooper, A. B. (1993) Hydroxylamine oxidoreductase from *Nitrosomonas europaea* is a multimer of an octa-heme subunit, *J. Biol. Chem. 268*, 14645−14654.
26. Arciero, D. M., Collins, M. J., Haladjian, J., Bianco, P., and Hooper, A. B. (1991) Resolution of the 4 hemes of cytochrome-c554 from *Nitrosomonas europaea* by redox potentiometry and optical spectroscopy, *Biochemistry 30*, 11459−11465.
27. Arciero, D. M., Balny, C., and Hooper, A. B. (1991) Spectroscopic and rapid kinetic-studies of reduction of cytochrome-c554 by hydroxylamine oxidoreductase from *Nitrosomonas europaea*, *Biochemistry 30*, 11466−11472.
28. Collins, M. J., Arciero, D. M., and Hooper, A. B. (1993) Optical spectropotentiometric resolution of the hemes of hydroxylamine oxidoreductase: Heme quantitation and pH-dependence of E(m), *J. Biol. Chem. 268*, 14655−14662.
29. Prince, R. C., and Hooper, A. B. (1987) Resolution of the hemes of hydroxylamine oxidoreductase by redox potentiometry and electron-spin-resonance spectroscopy, *Biochemistry 26*, 970−974.
30. Arciero, D. M., Golombeck, A., Hendrich, M. P., and Hooper, A. B. (1998) Correlation of optical and EPR signals with the P460 heme of hydroxylamine oxidoreductase from *Nitrosomonas europaea*, *Biochemistry 37*, 523−529.
31. Hendrich, M. P., Petasis, D., Arciero, D. M., and Hooper, A. B. (2001) Correlations of structure and electronic properties from EPR spectroscopy of hydroxylamine oxidoreductase, *J. Am. Chem. Soc. 123*, 2997−3005.
32. Popovic, D. M., Zaric, S. D., Rabenstein, B., and Knapp, E. W. (2001) Artificial cytochrome *b*: Computer modeling and evaluation of redox potentials, *J. Am. Chem. Soc. 123*, 6040−6053.
33. Mao, J., Hauser, K., and Gunner, M. R. (2003) How cytochromes with different folds control heme redox potentials, *Biochemistry 42*, 9829−9838.
34. Stephens, P. J., Jollie, D. R., and Warshel, A. (1996) Protein control of redox potentials of iron−sulfur proteins, *Chem. Rev. 96*, 2491−2513.
35. Simonson, T. (2001) Macromolecular electrostatics: Continuum models and their growing pains, *Curr. Opin. Struct. Biol. 11*, 243−252.
36. Rogers, N. K., and Moore, G. R. (1988) Spectroscopic identification of the heme ligands of cellobiose oxidase, *FEBS Lett. 228*, 69−73.
37. Wilson, G. S. (1974) Electrochemical studies of porphyrin redox reactions as cytochrome models, *Bioelectrochem. Bioenerg. 1*, 172−179.
38. Moore, G. R., and Pettigrew, G. W. (1990) Redox Potentials, in *Cytochromes c: Evolutionary, structural and physiological aspects*, pp 309−362, Springer, Berlin.
39. Bashford, D., and Karplus, M. (1991) Multiple-site titration curves of proteins: An analysis of exact and approximate methods for their calculation, *J. Phys. Chem. 95*, 9556−9561.
40. Antosiewicz, J., Mccammon, J. A., and Gilson, M. K. (1994) Prediction of pH-dependent properties of proteins, *J. Mol. Biol. 238*, 415−436.
41. Antosiewicz, J., Mccammon, J. A., and Gilson, M. K. (1996) The determinants of pK_as in proteins, *Biochemistry 35*, 7819−7833.
42. Georgescu, R. E., Alexov, E. G., and Gunner, M. R. (2002) Combining conformational flexibility and continuum electrostatics for calculating pK_as in proteins, *Biophys. J. 83*, 1731−1748.
43. Beroza, P., and Case, D. (1996) Including side chain flexibility in continuum electrostatic calculations of protein titration, *J. Phys. Chem. 100*, 20156−20163.
44. Sham, Y. Y., Muegge, I., and Warshel, A. (1998) The effect of protein relaxation on charge−charge interactions and dielectric constants of proteins, *Biophys. J. 74*, 1744−1753.
45. Mujica, V., Nitzan, A., Mao, Y., Davis, W., Kemp, M., and Ratner, M. A. (1999) Electron transfer in molecules and molecular wires: Geometry dependence, coherent transfer, and control, *Adv. Chem. Phys. 107*, 403−429.
46. Grabert, H., and Devoret, M. H. (1992) *Single Charge Tunneling: Coulomb Blockade Phenomena in Nanostructures*, Plenum, New York.
47. Upadhyay, A. K., Petasis, D. T., Arciero, D. M., Hooper, A. B., and Hendrich, M. P. (2003) Spectroscopic characterization and assignment of reduction potentials in the tetraheme cytochrome c_{554} from *Nitrosomonas europaea*, *J. Am. Chem. Soc. 125*, 1738−1747.
48. Rivera, M., Seetharaman, R., Girdhar, D., Wirtz, M., Zhang, X., Wang, X., and White, S. (1998) The reduction potential of cytochrome b_5 is modulated by its exposed heme edge, *Biochemistry 37*, 1485−1494.
49. Wirtz, M., Oganesyan, V., Zhang, X., Studer, J., and Rivera, M. (2000) Modulation of redox potential in electron-transfer proteins: Effects of complex formation on the active site microenvironment of cytochrome b_5, *Faraday Discuss. 116*, 221−234.
50. Marcus, R. A., and Sutin, N. (1985) Electron transfers in chemistry and biology, *Biochim. Biophys. Acta 811*, 265−322.
51. Bendall, D. S., Ed. (1996) *Protein Electron Transfer*, Bios Scientific Publishers, Oxford, U.K.
52. Balzani, V., Ed. (2001) *Electron Transfer in Chemistry*, Vols. 1−5, Wiley, Weinheim, Germany.

BI048060V